Magnetic and Structural Transitions in the Half-Doped Manganites $Pr_{0.5}Sr_{0.5-x}Ca_xMnO_3$

F. Damay, C. Martin,* A. Maignan, M. Hervieu, B. Raveau, Z. Jirak,† G. André,‡ and F. Bourée‡

Laboratoire CRISMAT, UMR 6508 associée au CNRS, ISMRA et Université de Caen 6, Boulevard du Maréchal Juin, 14050 Caen Cedex, France, Institute of Physics of ASCR, Cukrovarnicka 10, 16200 Prague, Czech Republic, and Laboratoire Léon Brillouin, CEA Saclay, 91191 Gif Sur Yvette, France

Received November 10, 1998
Revised Manuscript Received December 29, 1998

Introduction

The half-doped manganites with the perovskite structure, $Ln_{0.5}A_{0.5}MnO_3$, have been the purpose of numerous investigations, due to their interesting magnetic properties. The first studies were performed on $La_{0.5}Ca_{0.5}MnO_3$ by Wollan and Koehler[1] and by Goodenough,[2] who showed that the antiferromagnetic (AFM) structure of this material was CE-type and was associated with a 1:1 ordering of the Mn^{3+} and Mn^{4+} ions. The recent investigations of this phase by neutron diffraction and synchrotron radiation[3] and by electron microscopy[4] has allowed a complex ordering process to be evidenced. The manganite $Pr_{0.5}Sr_{0.5}MnO_3$, first studied by Knizek et al.,[5] has been the object of several studies[6−8] due to the discovery of colossal magnetoresistivity (CMR) in this material by Tomioka et al.[9] The comparison with $Pr_{0.5}Ca_{0.5}MnO_3$[10] shows the important role of the size of the A cation upon the magnetic and transport properties, as previously reported by various authors.[11,12] $Pr_{0.5}Sr_{0.5}MnO_3$ exhibits an A-type (Wollan and Koehler notation[1]) antiferromagnetic structure at low temperature, whereas $Pr_{0.5}Ca_{0.5}MnO_3$ is characterized by a CE-type antiferromagnetic structure and, contrary to $Pr_{0.5}Sr_{0.5}MnO_3$, does not show any CMR property up to 7 T. The structural behaviors of these phases are also very different. As T decreases, $Pr_{0.5}Ca_{0.5}MnO_3$ shows a transition from a classical $GdFeO_3$ type structure ($a_p\sqrt{2} \times 2a_p \times a_p\sqrt{2}$, space group (SG) *Pnma*, a_p referring to the cubic perovskite) to an incommensurate modulated structure ($(1/q)a_p\sqrt{2} \times 2a_p \times a_p\sqrt{2}$ with $q \cong 0.48$, SG *P*2/*m* or *Pmm*2) associated with a charge ordered state.[13] $Pr_{0.5}Sr_{0.5}MnO_3$ is characterized by a transition from a centered cell ($a_p\sqrt{2} \times a_p\sqrt{2} \times 2a_p$, SG *I*4/*mcm* or *I*2/*a*) to an F-type lattice ($2a_p \times 2a_p \times 2a_p$, SG *Fmmm* or *Fmm*2) and does not show any signature of charge ordering.[7,8]

The investigation of the oxide $Pr_{0.5}Sr_{0.41}Ca_{0.09}MnO_3$[14−16] showed that it exhibits better magnetoresistance properties than $Pr_{0.5}Sr_{0.5}MnO_3$ and evidenced two magnetic transitions from paramagnetic (PM) to ferromagnetic (FM) and from FM to AFM, at 250 and 180 K, respectively. The magnetic transitions temperatures are close to the two structural transitions ones, from *Imma* ($a_p\sqrt{2} \times 2a_p \times a_p\sqrt{2}$) to *I*4/*mcm* ($a_p\sqrt{2} \times a_p\sqrt{2} \times 2a_p$) and from *I*4/*mcm* (or *I*2/*a*) to *Pmmn* ($2a_p\sqrt{2} \times 2a_p \times a_p\sqrt{2}$), respectively, with decreasing temperature. The proof of the existence of Mn^{3+} and Mn^{4+} stripes in the low-temperature charge-ordered *Pmmn* structure was also given for the first time.

All these results suggest that the $Pr_{0.5}Sr_{0.5-x}Ca_xMnO_3$ system displays a great complexity, i.e. its average size of the A-site cations $\langle r_A \rangle$ governs the structural and physical properties. In the present paper, we establish the magnetic and structural phase diagrams of these half-doped manganites, and we study the relationships between their magnetic and structural transitions.

Experimental Section. The samples were prepared by solid-state reaction of Pr_6O_{11}, $SrCO_3$, CaO, and MnO_2, weighted in stoichiometric proportions, according to the sintering process previously reported.[8] The purity of the samples was first investigated using powder X-ray diffraction (XRD) and electron diffraction (ED). The crystallites were crushed in alcohol and the small flakes deposited on holey carbon films, supported by a copper grid. Diffraction characterization was carried out at room temperature (RT) and 92 K. The electron diffraction study as a function of temperature was made with a JEOL 2010 electron microscope. The ED patterns were recorded versus T, with a constant electron current density and increasing temperature from 92 to 300 K, the temperature being stabilized before each recording. The high-resolution electron microscopy was carried out with a TOPCON 002B, having a point resolution of 1.8 Å. The transmission electron microscopes were equipped with energy dispersive spectroscopy (EDS) analyzers. About 30 crystallites per sample were analyzed. This investigation showed that the actual compositions were very close to the nominal ones, within the limit of the accuracy of the technique. The results of the electron

† Institute of Physics of ASCR.
‡ Laboratoire Léon Brillouin.

(1) Wollan, E. O.; Koehler, W. C. *Phys. Rev.* **1955**, *100*, 545.
(2) Goodenough, J. B. *Phys. Rev.* **1955**, *100*, 564.
(3) Radaelli, P. G. ; Cox, D. E.; Marezio, M.; Cheong, S. W. *Phys. Rev. B* **1997**, *55*, 3015.
(4) Chen, C. H.; Cheong, S. W. *Phys. Rev. Lett.* **1996**, *76*, 4042.
(5) Knizek, K.; Jirak, Z.; Pollert, E.; Zounova, F. *J. Solid State Chem.* **1992**, *100*, 292.
(6) Argyriou, D. N.; Hinks, D. G.; Mitchell, J. F.; Potter, C. B.; Schultz, A. J.; Young, D. H.; Jorgensen, J. D.; Bader, S. D. *J. Solid State Chem.* **1996**, *124*, 381.
(7) Kawano, H.; Kajimoto, R.; Yoshizawa, H.; Tomioka, Y.; Kuwahara, H.; Tokura, Y. *Phys. Rev. Lett.* **1997**, *78*, 4253.
(8) Damay, F.; Martin, C.; Hervieu, M.; Maignan, A.; Raveau, B. *J. Magn. Magn. Mater.* **1998**, *184*, 71.
(9) Tomioka, Y.; Asamitsu, A.; Moritomo, Y.; Kuwahara, H.; Tokura, Y. *Phys. Rev. Lett.* **1995**, *74*, 5108.
(10) Jirak, Z.; Krupicka, S.; Simsa, Z.; Dlouha, M.; Vratislav, S. *J. Magn. Magn. Mater.* **1985**, *53*, 153.
(11) Hwang, H. Y.; Cheong, S. W.; Radaelli, P. G.; Marezio, M.; Battlog, P. *Phys. Rev. Lett.* **1995**, *75*, 914.
(12) Caignaert, V.; Maignan, A.; Raveau, B. *Solid State Commun.* **1995**, *95*, 957. Damay, F.; Martin, C.; Maignan, A.; Raveau, B. *J. Appl. Phys.* **1997**, *82*, 6181.
(13) Barnabé, A.; Hervieu, M.; Martin, C.; Maignan, A.; Raveau, B. *J. Appl. Phys.* **1998**, *84*, 5506.
(14) Wolfman, J.; Simon, Ch.; Hervieu, M.; Maignan, A.; Raveau, B. *J. Solid State Chem.* **1996**, *123*, 413.
(15) Laffez, P.; Van Tendeloo, G.; Millange, F.; Caignaert, V.; Hervieu, M.; Raveau, B. *Mater. Res. Bull.* **1996**, *31*, 905.
(16) Damay, F.; Jirak, Z.; Hervieu, M.; Martin, C.; Maignan, A.; Raveau, B.; André, G.; Bourée, F. *J. Magn. Magn. Mater.* **1998**, *190*, 221.

10.1021/cm981054z CCC: $18.00
Published on Web 02/25/1999

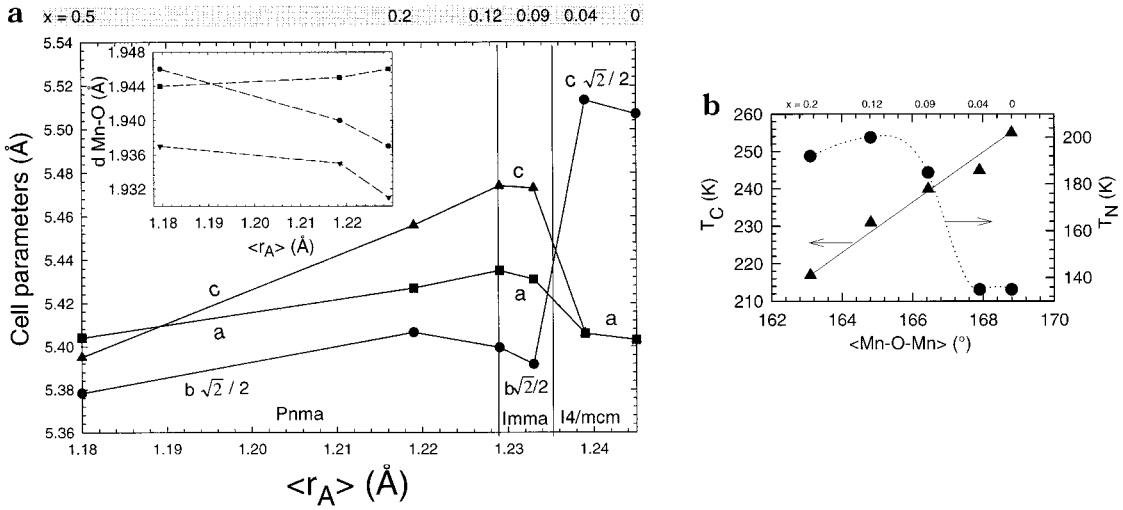

Figure 1. (a) $\langle r_A \rangle$ dependence of the cell parameters in the $Pr_{0.5}Sr_{0.5-x}Ca_xMnO_3$ series at room temperature, from NPD data. Inset: Mn−O distances vs $\langle r_A \rangle$, in the *Pnma* area. (b) $\langle$Mn−O−Mn$\rangle$ angle dependence of the Curie temperature (T_C) and of the Néel temperature (T_N) for samples of the $Pr_{0.5}Sr_{0.5-x}Ca_xMnO_3$ series. The crystallographic parameters have been determined by HRNPD data refinements, by assuming that the splitting of the oxygen sites express a local disorder, to obtain a better precision on the Mn−O distances and angles.

microscopy studies are not detailed in the present paper but only used for completing the structural description and solving specific problems.

Neutron experiments were carried out at LLB (Saclay, France) on the G41 diffractometer ($\lambda = 2.4266$ Å, 17° < 2θ < 97°) on eight compounds of the series, $Pr_{0.5}Sr_{0.5-x}Ca_xMnO_3$ ($x = 0$, 0.04, 0.09, 0.12, 0.15, 0.20, 0.30, and 0.50). Samples were first cooled to 2 K and patterns were recorded during warming from 2 K to room temperature. Additional high-resolution neutron powder diffraction (HRNPD) patterns were recorded at fixed temperature on the 3T2 diffractometer ($\lambda = 1.227$ Å, 6° < 2θ < 125°). Nuclear and magnetic structures were refined using the Fullprof program.[17]

The temperature dependence of the magnetization was registered with a vibrating sample magnetometer by warming the sample, previously zero-field-cooled, from 4.2 to 300 K in 100 G. The ac−χ curves were registered, after cooling in zero field, with $h_{ac} = 10$ Oe and $f = 33$ Hz.

Results and Discussion. *Structural Investigation at Room Temperature.* A preliminary NPD study, performed at room temperature, shows that the structural behaviors are strongly $\langle r_A \rangle$ dependent in the $Pr_{0.5}Sr_{0.5-x}Ca_xMnO_3$ series. In the paramagnetic state, three different space groups are observed, but the cell parameters remain those of a distorted perovskite, $\sim a_p\sqrt{2}$, $\sim 2a_p$, and $\sim a_p\sqrt{2}$ (Figure 1a). Upon increasing $\langle r_A \rangle$, the lattice evolves from a *Pnma* space group, for $0.5 \geq x \geq 0.15$, with octahedral tilt pattern of the $a^-b^+a^-$ kind (according to the Glazer notation[18]), to an *Imma* space group, for $0.15 > x \geq 0.09$, with the a^-0a^- tilt pattern. For $x = 0$ and 0.04, the room-temperature structure was solved from NPD data in the space group *I*4/*mcm* ($a_p\sqrt{2} \times a_p\sqrt{2} \times 2a_p$ cell) with the $00c^-$ tilt pattern;[8] the reflection conditions deduced from ED imply a different space group with a more complex tilt pattern. Among the possible space groups for this RT phase, *I*2/*a* (a monoclinic cell with $\beta \sim 90°$) is the only one compatible with both the NPD and ED data. Unfortunately, it is not possible to improve the structural refinement of the NPD data in this space group, because the cell distortion is too small. Nevertheless, the splitting of the oxygen site in the *I*4/*mcm* group results in a significant decrease of the agreement factors. The so-obtained average structure leads to an $(a^-a^-)c^-$ distortion (the notation in brackets is only used to indicate local disorder), which locally is compatible with the *I*2/*a* space group and suggests that this space group is the most probable. Nevertheless, to simplify the description of the crystallographic diagram the '*I*4/*mcm*' label will be retained in the present paper for this $(a^-a^-)c^-$ distortion. The structural transition from *P* to *I* versus $\langle r_A \rangle$ was investigated by ED and HREM, which provide information down to a few nanometers scale. This transition, which is clearly observed for $x \sim 0.15$, is not abrupt. A biphasic area is indeed observed over a small $\langle r_A \rangle$ range, close to this composition; the two *P*- and *I*-type structures coexist within a grain in the form of small domains. The tilting mode of the MnO_6 octahedra varies thus from 3D (*Pnma*) to 2D (*Imma*) and finally to 1D (*I*4/*mcm*) or from three-tilt to two-tilt and then to one-tilt systems, respectively.[19] A transition from a *P* group to an *I* one with increasing $\langle r_A \rangle$ has also been reported in other systems with large $\langle r_A \rangle$ values, for instance, $Pr_{1-x}Ba_xMnO_3$.[20] The room-temperature structural parameters, obtained from HRNPD refinements, are reported in Table 1 and the $\langle r_A \rangle$ dependence of the cell parameters is given in Figure 1a. $Pr_{0.5}Ca_{0.5}MnO_3$ is the only one which exhibits a pseudotetragonal compressed structure. Then, increasing $\langle r_A \rangle$ in the *Pnma* region increases the orthorhombic distortion of the compressed cell, in relation with a significant distortion of the MnO_6 octahedra (inset of Figure 1a). On the contrary, for larger $\langle r_A \rangle$ values, the structure is tetragonally elongated, the discontinuity between both tendencies occur-

(17) Rodriguez-Carvajal, J. *Collected Abstract of Powder Diffraction Meeting;* 1990, Galy, J., Ed.; Toulouse, France.
(18) Glazer, A. M. *Acta Crystallogr. B* **1972**, *28*, 3384.
(19) Woodward, P. M. *Acta Crystallogr. B* **1997**, *53*, 32.
(20) Jirak, Z.; Pollert, E.; Andersen, A. F.; Grenier, J. C.; Hagenmuller, P. *Eur. J. Solid State Inorg. Chem.* **1990**, *27*, 421.

Table 1. Crystallographic Data (from 3T2 NPD records) at 300 K, in the $Pr_{0.5}Sr_{0.5-x}Ca_xMnO_3$ System

x	$\langle r_A \rangle$ (Å) σ^2 (Å^2)	SG	a, b, c (Å)	V (Å^3)	Mn−O distances (Å)	Mn−O−Mn angles (deg)
0	1.245	*I*4/*mcm*	5.4031(1)	227.35	1.947(1) × 2	180.00
	$4.29 \cdot 10^{-3}$		7.7879(2)		1.927(1) × 4	164.80(4)
0.04	1.239	*I*4/*mcm*	5.4059(1)	227.85	1.949(1) × 2	180.00
	$4.25 \cdot 10^{-3}$		7.7968(2)		1.929(1) × 4	164.40(3)
0.09	1.233	*Imma*	5.4312(2)	226.65	1.928(1) × 2	162.85(10)
	$4.14 \cdot 10^{-3}$		7.6250(3)		1.938(1) × 4	167.95(6)
			5.4729(2)			
0.12	1.229	*Pnma*	5.4350(1)	227.21	1.931(1) × 2	162.74(6)
	$4.03 \cdot 10^{-3}$		7.6364(1)		1.937(1) × 2	166.90(3)
			5.4743(1)		1.946(1) × 2	
0.20	1.219	*Pnma*	5.4275(1)	226.40	1.935(1) × 2	162.05(3)
	$3.59 \cdot 10^{-3}$		7.6459(2)		1.940(1) × 2	164.17(3)
			5.4563(1)		1.945(1) × 2	
0.50	1.180	*Pnma*	5.4042(2)	221.77	1.937(1) × 2	158.07(14)
	$2.5 \cdot 10^{-7}$		7.6064(2)		1.946(1) × 2	157.92(11)
			5.3949(1)		1.944(1) × 2	

ring for $\langle r_A \rangle \sim 1.233$ Å. Consequently, the MnO_6 octahedron is slightly elongated for the compositions with larger $\langle r_A \rangle$ values and compressed for the smaller ones at room temperature. Note that, by increasing x, not only $\langle r_A \rangle$ decreases but also the variance σ^2, characteristic of the cationic A-site size mismatch[21] (Table 1 and ref 12).

The influence of $\langle r_A \rangle$ upon characteristic temperatures (Néel temperature, T_N; Curie temperature, T_C; and charge-ordering temperature, T_{CO}) is also interesting. According to magnetic measurements reported in a previous study,[11] T_C decreases with $\langle r_A \rangle$, because of the weakening of the electron-transfer interactions between manganese ions. In the $Pr_{0.5}Sr_{0.5-x}Ca_xMnO_3$ system, T_C decreases thus from 255 K for $\langle r_A \rangle = 1.245$ Å to 215 K for $\langle r_A \rangle = 1.219$ Å. Below $\langle r_A \rangle = 1.206$ Å, no long-range ferromagnetism is detected in the NPD patterns. With accurate refinements of the HRNPD patterns of the six compounds exhibiting a PM−FM transition, it is possible to link directly the linear decrease of T_C with $\langle r_A \rangle$—in the $\langle r_A \rangle$ range 1.245−1.219 Å—and thus with the decrease of the mean Mn−O−Mn angle in the structure (Figure 1b). The almost linear decrease of T_C (⟨Mn−O−Mn⟩), observed for compounds having similar A-site disorder values ($\sigma^2 \sim 4 \times 10^{-3}$ Å^2, Table 1), confirms the weakening of the DE interactions through the oxygen ion when ⟨Mn−O−Mn⟩ becomes smaller than 180°. In contrast, T_N goes through a maximum as the ⟨Mn−O−Mn⟩ angle varies as shown in Figure 1b. The different behaviors of T_N and T_C with $\langle r_A \rangle$ have motivated the following NPD investigation versus temperature.

Magnetic Phase Diagram. The magnetic phase diagram, deduced from NPD data, established in the ($\langle r_A \rangle$, T) plane (Figure 2a) in the range 2−300 K, is complex. It allows several magnetic regions to be distinguished and, in particular, four monophasic regions (two AFM, one PM, one FM). The two AFM regions observed at low temperature in the range from 2 to 120−170 K belong to the CE-type and to the A-type structures. The CE-type AFM region extends over a rather broad region, with $\langle r_A \rangle$ ranging from 1.18 to 1.233 Å ($0.09 \leq x \leq 0.50$), whereas the A-type area, observed for a larger A cation, is limited to a very narrow region, 1.233 Å $< \langle r_A \rangle \leq 1.245$ Å (corresponding to $0 \leq x < 0.09$). The FM state is only observed for $\langle r_A \rangle$ values larger than 1.206 Å ($0 \leq x < 0.30$), and the temperature range where it exists increases as $\langle r_A \rangle$ increases. In the CE-type AFM area, nuclear superstructure peaks appear on the NPD pat-

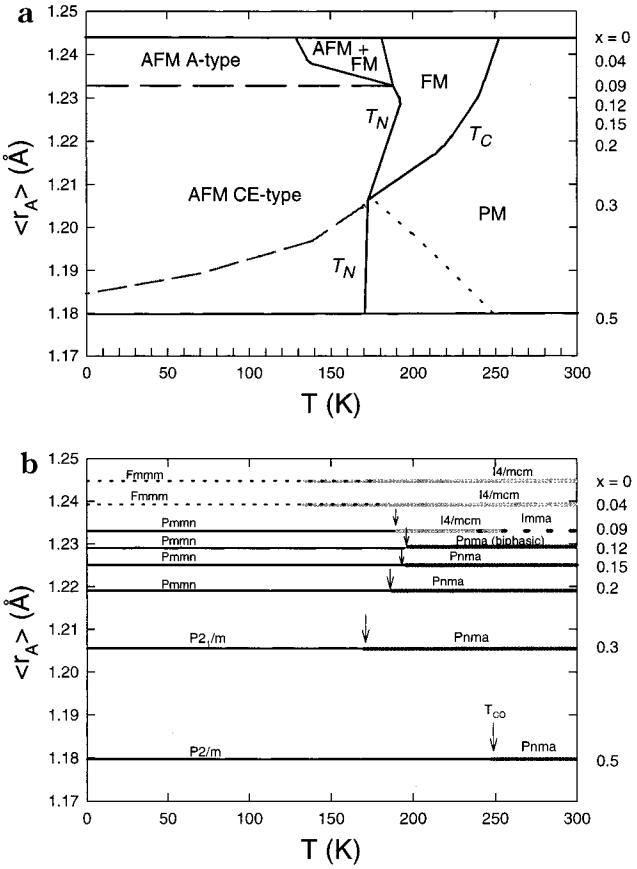

Figure 2. (a) Schematic ($\langle r_A \rangle$ (or x), T) magnetic diagram. The full lines separate the different magnetic regions, whereas the dashed and dotted line, established from the ac−χ curves, correspond to the variation of the magnetic fluctuations in the AFM and paramagnetic areas, respectively. (b) T dependence of the crystallographic parameters of the $Pr_{0.5}Sr_{0.5-x}Ca_xMnO_3$ samples. The eight horizontal lines correspond to the different samples that have been studied; their calcium content, x, is labeled on the right y-scale and their average A-site ionic radius on the left y-axis. The small vertical arrows indicate the CO temperature below which superstructure peaks are observed on NPD patterns. The $P2_1/m$ and $P2/m$ space group for $x = 0.3$ and 0.5 at low temperature have been determined by ED.

(21) Rodriguez-Martinez, L. M.; Attfield, J. P.*Phys. Rev. B* **1996**, *54*, R15622.

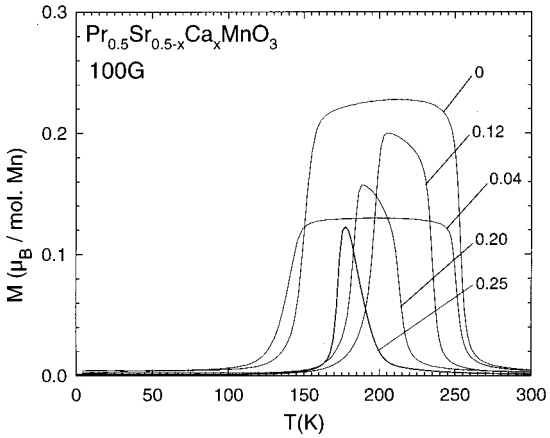

Figure 3. *T* dependence of the magnetization registered in 100 G after a zero-field-cooling process. Ca (*x*) contents in $Pr_{0.5}Sr_{0.5-x}Ca_xMnO_3$ are labeled on the graph.

terns below the charge-ordering temperature T_{CO} (see arrows on Figure 2b). Note that two kinds of samples can be distinguished. In the composition range $0.09 \leq x < 0.3$, i.e., samples exhibiting a FM state, T_{CO} and T_N coincide ($T_{CO} = T_N$), whereas for $0.3 \leq x \leq 0.5$, T_{CO} is always higher than T_N.

In summary, according to the size of the A-site cations, the magnetic phase diagram, deduced from NPD data, shows three different kinds of magnetic transitions:

(i) For smaller $\langle r_A \rangle$ values corresponding to $0.30 \leq x \leq 0.50$, i.e., $1.18 \leq \langle r_A \rangle \leq 1.206$ Å, a single magnetic transition from the PM to the CE-type AFM states is observed. In this region, T_N does not vary significantly with $\langle r_A \rangle$, $T_N \cong 170$ K.

(ii) For intermediate $\langle r_A \rangle$ values corresponding to $0.09 \leq x < 0.30$, i.e., 1.206 Å $< \langle r_A \rangle \leq 1.233$ Å, two magnetic transitions are observed successively with decreasing temperature, PM to FM and FM to CE-type AFM.

(iii) For the larger $\langle r_A \rangle$ values characterized by an A-type AFM structure, there is still a PM−FM transition followed by a FM−AFM one, but the latter is progressive and the coexistence of two magnetic phases is observed in a temperature range of about 50 K.

At this point of the investigations, it is of interest to complete the magnetic phase diagram (Figure 2a) on the basis of ac susceptibility and dc magnetization measurements, although these techniques do not allow us to distinguish the A-type from the CE-type antiferromagnetic states. The $M(T)$ curves registered under 100 G, on warming after zero-field cooling (Figure 3), show indeed that the "pulse-shaped" curves characteristic of the AFM−FM−PM transitions are observed for the CE-type AFM state ($0.09 \leq x < 0.30$) as well as for the A-type AFM state ($0 \leq x < 0.09$). Note that the magnetic transition temperatures, T_N and T_C, measured at the inflection points on the left and right branches of the curves, coincide perfectly with those deduced from the NPD data. In contrast, the ac−$\chi(T)$ curves, registered for $0.30 \leq x \leq 0.50$ (Figures 4−6), show that the magnetic behavior in this composition range is more complex than the single AFM−PM transition expected from the NPD data. In the absence of long-range ferromagnetism, the ac−χ technique has been shown to be very sensitive to the change of magnetic fluctuations from FM above T_{CO} to AFM below, as previously

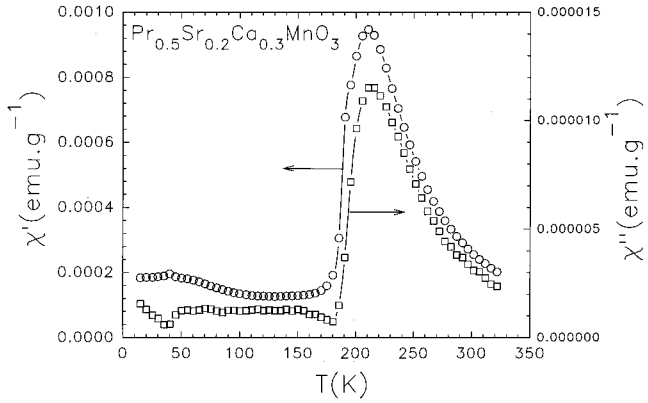

Figure 4. *T* dependent real-part (χ', left *y*-axis) and imaginary-part (χ'', right-axis) of the magnetic susceptibility of $Pr_{0.5}Sr_{0.2}Ca_{0.3}MnO_3$ ($x = 0.3$).

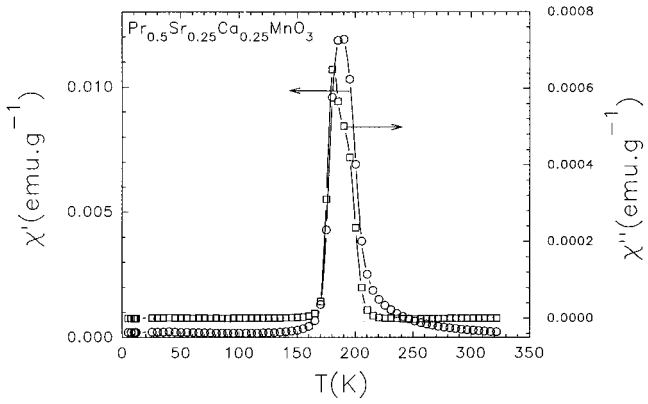

Figure 5. $\chi'(T)$ and $\chi''(T)$ curves of $Pr_{0.5}Sr_{0.25}Ca_{0.25}MnO_3$ ($x = 0.25$).

reported for $Ca_{1-x}Bi_xMnO_3$.[22] Consequently, a bump at T_{CO} is clearly observed on ac−χ curves for $0.30 \leq x \leq 0.50$ in $Pr_{0.5}Sr_{0.5-x}Ca_xMnO_3$, T_{CO} ranging from ∼190 to ∼250 K as *x* increases. Thus, this technique appears to be more sensitive to the magnetic fluctuations rather than to the long-range AFM state evidenced by NPD, since no special feature can be detected on the ac−χ curves at T_N. This is clearly shown for $Pr_{0.5}Ca_{0.5}MnO_3$, with a bump on the $\chi(T)$ curve (Figure 6a) at $T_{CO} = 250$ K, in good agreement with NPD results, but without any special feature at $T_N = 170$ K (NPD). The dotted line in the paramagnetic zone (PM) on Figure 2a represents the change of the magnetic fluctuations from FM to AFM with decreasing temperature. $\chi'(T)$ and $\chi''(T)$ curves of the limit compound $Pr_{0.5}Sr_{0.2}Ca_{0.3}MnO_3$ ($x = 0.30$) (Figure 4) indicate that this oxide still exhibits ferromagnetic interactions above $T_N \sim T_{CO} \sim 180$ K. Nevertheless, the maximum value of χ' (9×10^{-4} emu·g^{-1}) is very small compared to that of $Pr_{0.5}Sr_{0.25}Ca_{0.25}MnO_3$ ($x = 0.25$), $\chi'_{max} = 1.2 \times 10^{-2}$ emu·g^{-1} (Figure 5), so these FM interactions cannot be detected on NPD patterns for $x = 0.30$. This is also consistent with the $\chi''(T)$ shape, which is very sharp at T_C for $x = 0.25$ but very broad for $x = 0.30$, suggesting that, for the latter phase, ferromagnetism results only from strong FM fluctuations above T_{CO}. It is remarkable that the FM fluctuations are also observed as *x* increases, i.e., as $\langle r_A \rangle$ decreases as shown for instance for the

(22) Bao, W.; Axe, J. D.; Chen, C. H.; Cheong, S. W. *Phys. Rev. Lett.* **1997**, *78*, 543.

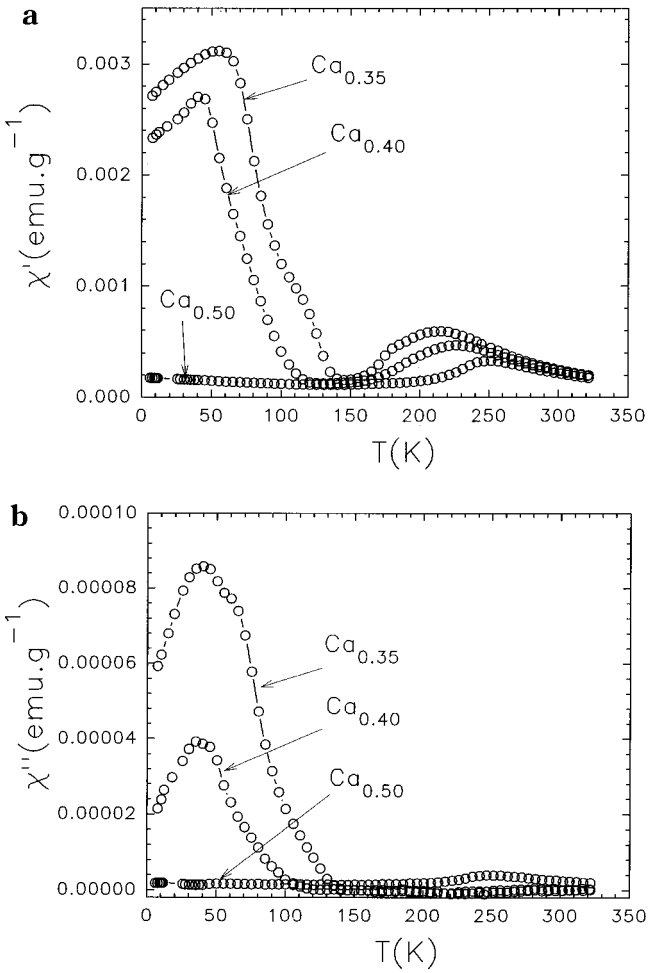

Figure 6. (a) $\chi'(T)$ curves of three $Pr_{0.5}Sr_{0.5-x}Ca_xMnO_3$ samples ($x = 0.35$, 0.45 and 0.50). (b) Corresponding $\chi''(T)$ curves.

compositions $x = 0.35$ and 0.40, for which these fluctuations occur below T_{CO}, χ' reaching 3.2×10^{-3} emu·g^{-1} at 50 K for $x = 0.35$. They finally totally disappear for $x = 0.5$ (Figure 6a). The existence of these ferromagnetic fluctuations in the AFM CE-type region for this composition range can also be evidenced from the $\chi''(T)$ curves of the $x = 0.35$ and $x = 0.40$ compounds (Figure 6b). A new characteristic temperature, below which these fluctuations appear, can thus be determined on each of these ac−χ curves. They correspond to the dashed line inside the CE-type AFM region (Figure 2a). This line seems to be a continuation of the T_C ($\langle r_A \rangle$) line obtained from the larger sizes, i.e., $0 \leq x < 0.3$ (solid line in Figure 2a).

Structural Transitions and Charge Ordering. The knowledge of the relationships between structural and magnetic transitions is very important for understanding the physics in these half-doped manganites. The crystallographic phase diagram of the $Pr_{0.5}Sr_{0.5-x}Ca_xMnO_3$ system, in the ($\langle r_A \rangle$, T) plane, although very complex (Figure 2b), exhibits similarities with the magnetic phase diagram (Figure 2a).

For $0 \leq x < 0.09$, corresponding to large $\langle r_A \rangle$ values between 1.245 and 1.233 Å, only one structural transition is observed, characterized by two monophasic areas separated by a biphasic one. The region of the low-temperature phase coincides exactly with the A-type AFM area. The nuclear structure of this A-type AFM oxide can be perfectly refined in the "$2a_p \times 2a_p \times 2a_p$" centrosymmetric space group $Fmmm$ previously reported for $Pr_{0.5}Sr_{0.5}MnO_3$ ($x = 0$).[8] The fact that this cell exhibits a single crystallographic Mn-site suggests that it is not charge-ordered. Nevertheless, the corresponding noncentrosymmetric space group $Fmm2$, which contains two distinct Mn sites, cannot be ruled out, so the ambiguity about the existence of charge ordering in this temperature range cannot be removed. A convergent beam electron diffraction study is in progress in order to attempt to solve this point. The region of the high-temperature phase covers both the PM and FM areas, so no phase transition accompanies the PM−FM transition; it is even remarkable that the cell parameters do not vary at the transition.[8] The biphasic zone coincides exactly with the one observed on the magnetic phase diagram, that is, in this region, the I phase is ferromagnetic, whereas the F phase is A-type antiferromagnetic. These results show that, for larger A cations, the FM−AFM transition is closely related to a structural transition, whereas the PM−FM transition does not affect the structure. This last point is reinforced by the structural study carried out by X-ray powder diffraction on $Pr_{0.5}Sr_{0.5}MnO_3$ from 300 to 500 K. It shows a transition from the $I4/mcm$ to an $Imma$ cell occurring in the temperature range 380−410 K, i.e., totally decoupled from the PM−FM transition. Results from refinement of the HRNPD pattern recorded at 500 K[23] evidence, for the $Imma$ form at 500 K, a flattened MnO_6 octahedron which is more regular than in the $I4/mcm$ form at 292 K, where the octahedron is elongated.[8] The $Imma$−$I4/mcm$ transition is similar for $Pr_{0.5}Sr_{0.5}MnO_3$ and $Pr_{0.5}Sr_{0.41}Ca_{0.09}MnO_3$; it goes with a reorientation of the crystallographic axes. Moreover, it is clear that the structural transition is not linked to the PM−FM transition, since they occur at 395 and 280 K respectively in $Pr_{0.5}Sr_{0.5}MnO_3$.

For $0.09 \leq x < 0.50$, the first important feature deals with the appearance of charge ordering (CO) at low temperature. The comparison of the magnetic (Figure 2a) and structural (Figure 2b) diagrams shows that T_{CO} coincides with T_N in the range 0.09−0.30. In contrast, for $0.30 < x \leq 0.50$, T_{CO} is significantly larger than T_N and increases as $\langle r_A \rangle$ decreases, whereas T_N remains constant. The CO phases are all characterized by the existence of extra reflections which are clearly observed in the low-temperature ED patterns. For the whole area, except for the limit compounds, $x = 0.5$, the satellites are in commensurate positions, involving a doubling of the a parameter. Here again, at low temperature, a structural transition is observed vs $\langle r_A \rangle$, from a $Pmmn$-type supercell for $x = 0.09$ to a $P2_1/m$-type supercell[3] for $0.2 < x < 0.5$. Both commensurate structures can be described from alternation, along $\vec{a}$, of (100) stripes of distorted Mn^{3+} octahedra and (100) stripes of almost regular Mn^{4+} octahedra. An important remark is that the commensurate character of the CO does not depend on the space group. However, the two types of CO differ by their establishment vs T. The $Pmmn$-type exhibits an abrupt transition at T_{CO}, whereas the $P2_1/m$-type exhibits a broad transition with the stabilization of different incommensurate modulations ($a = 1/q \cdot a_p\sqrt{2}$ with $q < 0.5$) just below T_{CO}. The low-temperature form of $Pr_{0.5}Ca_{0.5}MnO_3$ is incommensurate with $q = 0.48$ (SG

(23) Damay, F., Ph.D. Thesis, Caen University, 1998.

*P*2/*m*). This particular behavior has been previously attributed to a tiny deviation from 1 of the Mn^{3+}/Mn^{4+} ratio.[13]

Conclusions. This study shows the great complexity of the structural transitions in the $Pr_{0.5}Sr_{0.5-x}Ca_xMnO_3$ system and the possible relationships with the magnetic ones. The most important point concerns the relationships between charge ordering and magnetism. In this respect, the following points must be emphasized:

(i) As expected, T_C is regularly reduced as $\langle r_A \rangle$ is decreased from $Pr_{0.5}Sr_{0.5}MnO_3$ to $Pr_{0.5}Ca_{0.5}MnO_3$. However, a long-range-ordered ferromagnetic state is confirmed only for the composition range from $Pr_{0.5}Sr_{0.5}MnO_3$ to $Pr_{0.5}Sr_{0.25}Ca_{0.25}MnO_3$, for which $T_C > T_N$. The FM state hinders the CO process, when it exists, so that $T_{CO} = T_N$ from $Pr_{0.5}Sr_{0.41}Ca_{0.09}MnO_3$ to $Pr_{0.5}Sr_{0.2}Ca_{0.3}MnO_3$. For these compounds, T_N does not evolve regularly, since T_N first increases from 135 K for $Pr_{0.5}Sr_{0.5}MnO_3$ to 190 K for $Pr_{0.5}Sr_{0.38}Ca_{0.12}MnO_3$ and then decreases to 175 K for $Pr_{0.5}Sr_{0.25}Ca_{0.25}MnO_3$.

(ii) For compositions corresponding to $\langle r_A \rangle$ values smaller or equal to that of $Pr_{0.5}Sr_{0.2}Ca_{0.3}MnO_3$, long-range FM is suppressed if one refers to NPD. Concomitantly, the CO is reinforced as shown from the increase of T_{CO} values from 180 to 250 K for $x = 0.25$ and 0.30 compositions, respectively. Nevertheless, T_N keeps a rather constant value in these compounds with $T_N \ll T_{CO}$, so that a clear decoupling of the CO ordering and long-range spin ordering occurs.

(iii) Although no FM is deduced from the NPD study in the 1.18 Å $< \langle r_A \rangle <$ 1.206 Å range, ac−χ measurements clearly indicate the existence of, at least, ferromagnetic fluctuations below T_{CO}. In this region (from $x = 0.30$ to 0.50), T_C keeps following the aforementioned evolution, i.e., T_C still decreases with $\langle r_A \rangle$. The corresponding compounds are thus characterized by transition temperatures with $T_{CO} > T_N > T_C$.

(iv) The best CMR properties in this series have been reported for $Pr_{0.5}Sr_{0.41}Ca_{0.09}MnO_3$.[14] This compound is the first one, by decreasing $\langle r_A \rangle$ in the $Pr_{0.5}Sr_{0.5-x}Ca_xMnO_3$ system, which shows a charge-ordered CE-type AFM structure at low temperature and still exhibits a high T_C. One can thus assume that its remarkable CMR properties are related to the fact that its insulating charge-ordered AFM state is the most metastable of the series and can be easily collapsed into a FM metallic one by magnetic field application.

Acknowledgment. The authors thank Dr R. Retoux (Laboratoire des Fluorures, Université du Maine, 72017 Le Mans Cedex, France) for X-ray records in the temperature range 300−500 K.

CM981054Z